Inorganic Chemistry

Article

Cite This: Inorg. Chem. 2018, 57, 5292−5298

pubs.acs.org/IC

In Situ X-ray Diffraction Study of the Thermal Decomposition of Selenogallates $Cs_2[Ga_2(Se_2)_{2-x}Se_{2+x}]$ (x = 0, 1, 2)

Daniel Friedrich, Marc Schlosser, Christian Näther,† and Arno Pfitzner*

Institut für Anorganische Chemie, Universität Regensburg, Universitätsstraße 31, 93040 Regensburg, Germany

Supporting Information

ABSTRACT: The selenogallates $CsGaSe_3$ and $Cs_2Ga_2Se_5$ release gaseous selenium upon heating. An in situ high-temperature X-ray powder diffraction analysis revealed a two-step degradation process from $CsGaSe_3$ to $Cs_2Ga_2Se_5$ and finally to $CsGaSe_2$. During each step, one Se_2^{2-} unit of the anionic chains in $Cs_2[Ga_2(Se_2)_{2-x}Se_{2+x}]$ (x = 0, 1, 2) decomposes, and one equivalent of selenium is released. This thermal decomposition can be reverted by simple addition of elemental selenium and subsequent annealing of the samples below the decomposition temperature. The influence of the diselenide units in the anionic selenogallate chains on the optical properties and electronic structures was further studied by UV/vis diffuse reflectance spectroscopy and relativistic density functional theory calculations, revealing increasing optical band gaps with decreasing Se_2^{2-} content.

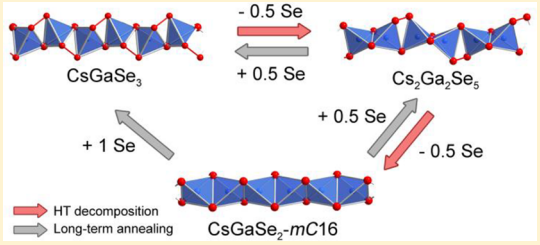

INTRODUCTION

Chalcogenometallates of the group 13 metals with alkali metal cations $M_xT_yQ_z$ (M = alkali metal, T = triel, Q = chalcogen) as counterions are an interesting class of compounds due to their semiconducting properties.[1,2] The crystal structures of compounds in the ternary systems $M-T-Q$ mostly consist of anionic structures of connected TQ_4^{5-} tetrahedra in a surrounding of alkali metal cations. Condensation of these tetrahedral building units leads to the formation of more complex oligomeric or polymeric one-, two- or three-dimensional chalcogenotrielate anions. Even though most crystalline phases in these systems contain the elements in their most stable oxidation states, a small number of mixed-valent indates[3] and compounds containing polychalcogenide units are known.[4−16] Incorporation of such polychalcogenide units into the anionic structures leads to the formation of more complex, uncommon one-dimensional structures like $CsGaQ_3$,[4,5] $Cs_2Ga_2Q_5$,[6,7] $CsAlTe_3$,[8] several *per*chalcogenoborates[9−11] and -antimonates,[12−15] or the neutral chains in P_2S_7.[16] The polychalcogenide units Q_2^{2-} or Q_3^{2-} in such compounds have a significant influence on the semiconducting properties of these substances.[17]

We recently reported on our investigations of ternary thiogallates $CsGaS_3$,[5] $Cs_2Ga_2S_5$,[6] and $CsGaS_2$.[18,19] The crystal structures of these compounds contain anionic chains $^1_\infty[Ga_2(S_2)_{2-x}S_{2+x}^{2-}]$ (x = 0, 1, 2), which release gaseous sulfur upon heating due to decomposition of the disulfide units.[17] An in situ high-temperature X-ray diffraction analysis of this process revealed a stepwise degradation from $CsGaS_3$ to $Cs_2Ga_2S_5$ to $CsGaS_2$-*mC*16. During each step, one S_2^{2-} unit of the anionic chains decomposes, and one equivalent of gaseous sulfur is released. While the thermal process is irreversible, $CsGaS_3$ and $Cs_2Ga_2S_5$ can be recovered from both polymorphs of $CsGaS_2$ by using cesium polysulfide fluxes.

Herein, we report on the analysis of the phase changes in the corresponding selenides $CsGaSe_3$ and $Cs_2Ga_2Se_5$, which also decompose upon heating. These decomposition reactions were further studied in situ using X-ray powder diffraction at lab sources, with synchrotron radiation, and thermogravimetric analyses. Like the analogous system $Cs_2[Ga_2(S_2)_{2-x}S_{2+x}^{2-}]$ (x = 0, 1, 2), the selenides should also exhibit a trend of decreasing optical band gaps with increasing Se_2^{2-} content. Due to the overall smaller band gaps of the selenides and the potential to absorb visible light contrary to the UV absorbing sulfides, these materials could be interesting for several applications, e.g. chemical photocatalysis. To study the optical properties, the compounds were studied by UV/vis diffuse reflectance spectroscopy. For the interpretation of the results, a combination of ab initio density functional theory (DFT) calculations and Raman spectroscopy was used.

RESULTS AND DISCUSSION

The crystal structures of $CsGaSe_3$,[4] $Cs_2Ga_2Se_5$,[7] and $CsGaSe_2$-*mC*16[20,21] feature polymeric, anionic chalcogenogallate chains $^1_\infty[Ga_2(Q_2)_{2-x}Q_{2+x}^{2-}]$ (Q = S, Se; x = 0, 1, 2) like the analogous sulfides, see Figure 1. $CsGaSe_2$ crystallizes in two polymorphic modifications with $CsGaSe_2$-*mC*16 being the high-temperature polymorph and $CsGaSe_2$-*mC*64 being the low-temperature polymorph.[21] The Pearson symbols (-*mC*64/-*mC*16), stating the crystal system, centering, and number of atoms per unit cells, are used to differentiate between both crystalline modifications throughout this publication. Crystallographic

Received: February 5, 2018
Published: April 18, 2018

DOI: 10.1021/acs.inorgchem.8b00324
Inorg. Chem. 2018, 57, 5292−5298

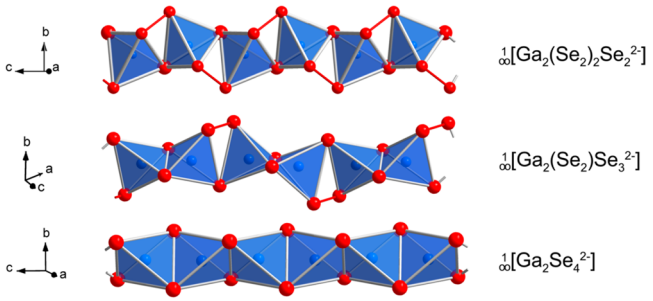

Figure 1. Sections of the selenogallate chains $^1_\infty[Ga_2(Se_2)_{2-x}Se_{2+x}^{2-}]$ (x = 0, 1, 2) in $CsGaSe_3$, $Cs_2Ga_2Se_5$, and $CsGaSe_2$-$mC16$.

data for the selenides are listed in Table 1. These chains can be converted into each other by substituting the Q_2^{2-} units with

Table 1. Crystallographic Data of $CsGaSe_2$-$mC64$,[21] $CsGaSe_2$-$mC16$,[21] $Cs_2Ga_2Se_5$,[7] and $CsGaSe_3$[4] at Ambient Conditions (X-ray Powder Diffraction Data, Cu Kα_1 Radiation, 20 °C)

	$CsGaSe_2$-$mC64$	$CsGaSe_2$-$mC16$	$Cs_2Ga_2Se_5$	$CsGaSe_3$
crystal system		monoclinic		
space group	$C2/c$	$C2/c$	$C2/c$	$P2_1/c$
a/Å	11.048(1)	7.650(1)	15.468(1)	7.662(1)
b/Å	11.057(1)	12.546(1)	7.411(1)	12.989(1)
c/Å	16.830(1)	6.170(1)	13.012(1)	6.710(1)
β/°	99.404(1)	113.462(4)	126.524(1)	106.046(5)
V/Å^3	2028.33(3)	543.22(6)	1198.63(3)	641.80(7)
Z	16	4	4	4

normal-valent Q^{2-} anions. In all these compounds, the cesium cations form a cubic diamond analogous topology. Even though the anionic chains in the respective selenides and sulfides are identical, only $CsGaQ_3$ and $CsGaQ_2$-$mC16$ (Q = S, Se) are isotypic. The main difference in the compounds $Cs_2Ga_2Q_5$ is the orientation of the anionic chains $^1_\infty[Ga_2(Q_2)Q_3^{2-}]$. In $Cs_2Ga_2S_5$, the thiogallate chains run along the 001, while the selenogallate chains in $Cs_2Ga_2Se_5$ run along the 101 direction. The low-temperature polymorph $CsGaSe_2$-$mC64$ has a two-dimensional layered structure of corner sharing Ga_4Se_{10} supertetrahedra and is not structurally related to the three different one-dimensional phases.[21]

We recently showed that the sulfides can be degraded starting stepwise from $CsGaS_3$ to $Cs_2Ga_2S_5$ and finally to $CsGaS_2$ when thermally exposed due to subsequent decomposition of the disulfide units. The high-temperature behavior of the corresponding selenides is similar, yet different. Similar to the analogous sulfides $CsGaS_3$ and $Cs_2Ga_2S_5$, the release of gaseous chalcogen can be observed upon heating of $CsGaSe_3$ and $Cs_2Ga_2Se_5$. To gain further insight into these processes, powdered samples of the selenides were studied in situ using high-temperature X-ray diffraction techniques. Besides the thermal degradation, we also investigated the possibility of a reselenation, i.e., the controlled (and stepwise) reinsertion of selenium into the selenium-poor phases.

Thermal Decomposition of One-Dimensional Selenogallates. *High-Temperature in Situ X-ray Diffraction.* No change in the diffraction pattern of $CsGaSe_3$, aside from the temperature induced shift of all reflections toward smaller diffraction angles, can be observed up to about 540 °C, see Figure 2. The diffraction pattern then suddenly changes at temperatures above 540 °C, and the resulting crystalline phase

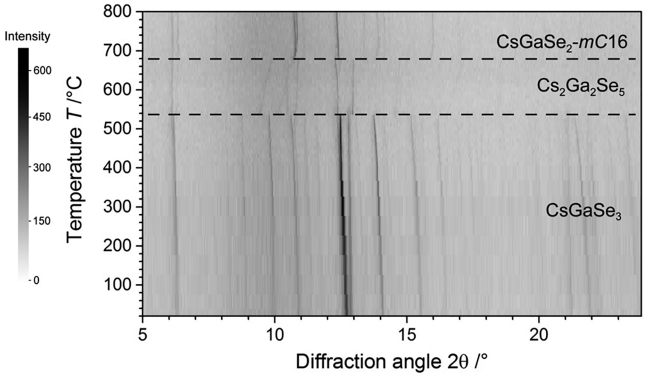

Figure 2. Evolution of the X-ray powder diffraction pattern during the thermal degradation of $CsGaSe_3$ in the temperature region from 20–800 °C (Mo Kα_1 radiation; λ = 0.709300 Å).

was identified as $Cs_2Ga_2Se_5$. At 680 °C, another sudden change in the diffraction pattern was observed. Above this temperature, the high-temperature polymorph $CsGaSe_2$-$mC16$ is the only crystalline phase that can be detected. The low-temperature polymorph $CsGaSe_2$-$mC64$ could not be detected because the final step occurs above the phase-transition temperature of $CsGaSe_2$-$mC64$ (T_{trans} = 610 °C). Thus, the degradation behavior of $CsGaSe_3$ is identical to that of $CsGaS_3$, while the temperatures for the first and the second step are 440 °C (first step) and 540 °C (second step) for the sulfide system.

A similar in situ high-temperature X-ray analysis of $Cs_2Ga_2Se_5$ on our in-house diffractometer also revealed $CsGaSe_2$-$mC16$ as the final crystalline product phase of this degradation. However, we observed several distinct temperature ranges of intermediate crystalline phases in the course of this reaction. Initial attempts to refine the crystal structures of these intermediates by Rietveld methods failed, likely due to the relatively high absorption of the powdered sample (μ(Mo Kα_1) = 26 mm^{-1}), fluorescence due to selenium when using Mo-radiation, and poor crystallinity of the samples. Usage of Cu radiation lead to increased absorption (μ(Cu Kα_1) = 70 mm^{-1}) and very long measurement times, which prevents an investigation of this dynamic process. To fully elucidate this decomposition reaction including the intermediate phases, we performed the experiment using synchrotron radiation of a suitable custom wavelength (λ = 0.399949 Å) at the ID-22 beamline of the European Synchrotron Research Facility (ESRF). These measurements (Figure 3) revealed that in fact, no unknown intermediate phases exist in the course of the decomposition of $Cs_2Ga_2Se_5$. At temperatures above 240 °C, the first new crystalline phase was identified as the low-temperature polymorph $CsGaSe_2$-$mC64$ from the diffraction data. The decomposition of $Cs_2Ga_2Se_5$ was completed at 380 °C, and $CsGaSe_2$-$mC64$ remained as the sole crystalline phase. At 600 °C, $CsGaSe_2$-$mC64$ undergoes a polymorphic phase transition to $CsGaSe_2$-$mC16$, which was already studied in an earlier publication.[21] The differing results from our in-house experiments and the synchrotron measurements can be explained by the different experimental setups. Due to the very rapidly spinning capillary and a hot air blower used at ID-22, a homogeneous temperature distribution in the whole powdered phase inside the capillary can be assured. Contrary,

DOI: 10.1021/acs.inorgchem.8b00324
Inorg. Chem. 2018, 57, 5292–5298

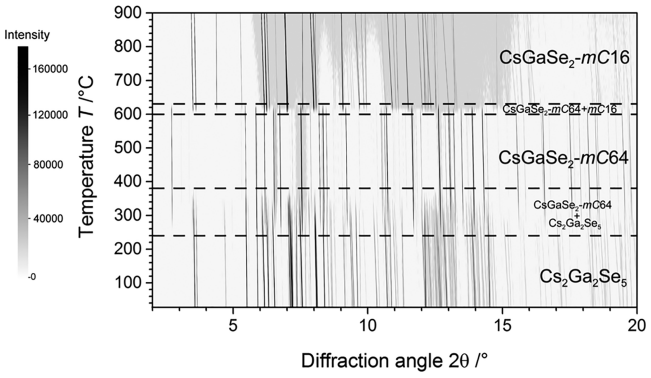

Figure 3. Evolution of the X-ray powder diffraction pattern during the thermal degradation of $Cs_2Ga_2Se_5$ in the temperature region from 20–900 °C (ESRF ID-22; λ = 0.399949 Å).

the slowly rotating capillary is heated indirectly by a graphite furnace which apparently leads to an inhomogeneous temperature distribution inside the STOE capillary furnace. While the different high-temperature equipment does not significantly influence the starting temperature of the decomposition, significant discrepancies in the course of the reaction are observed. Using our knowledge from the synchrotron experiments, a subsequent analysis of our in-house experiments revealed that all reflections can indeed be attributed to $Cs_2Ga_2Se_5$ and the two different polymorphs of $CsGaSe_2$. Significant differences of the reflection intensities by severe texture effects combined with the slow progress of the reaction apparently lead to diffraction patterns which were difficult to interpret.

The differing thermal stability of freshly prepared samples of $Cs_2Ga_2Se_5$ compared to the intermediate phase in the course of the decomposition of $CsGaSe_3$ can be explained as follows. Our investigations of the crystal structures of $Cs_2Ga_2Se_5$ revealed a disorder of the Se_2^{2-} units in the anionic chains. Samples of $Cs_2Ga_2Se_5$ obtained after long-term annealing have a high degree of crystallinity, and the diselenide units in the anionic chains are well ordered. The intermediate phase $Cs_2Ga_2Se_5$ observed during the decomposition of $CsGaSe_3$ is supposed to have a significantly lower crystallinity as well as a high degree of disorder of the diselenide dumbbells within single strands and also severe disorder present in different strands. This disorder and low crystallinity lead to the overall low diffraction intensities of $Cs_2Ga_2Se_5$ as well as the significant shifts of several reflections, indicating a massive structural rearrangement in this phase. Due to the reconstructive character of this reaction, the further degradation of $Cs_2Ga_2Se_5$ can therefore be described as kinetically hindered until a certain time necessary for the rearrangement of the phase has passed. Only the high-temperature polymorph $CsGaSe_2$-*mC*16 is observed after a second reconstructive phase transition due to the fact that the decomposition temperature is already above the phase-transition temperature of 610 °C. It should also be noted that the observed reflection intensities of $Cs_2Ga_2Se_5$ are significantly lower than those of the two other crystalline phases. Furthermore, the intermediate phase shows severe shifts of several reflections, which can be attributed to the rearrangement of the atoms during this topotactic process.

Thermogravimetric Analysis. The thermal decomposition of $CsGaSe_3$ and $Cs_2Ga_2Se_5$ was also studied by using thermogravimetric analysis (Figure 4). The observed mass losses for $CsGaSe_3$ (15.8%; calcd 18.0%) and $Cs_2Ga_2Se_5$ (7.4%;

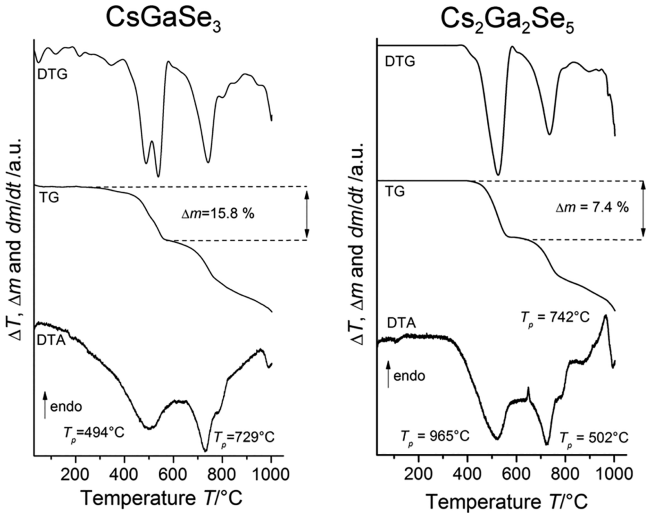

Figure 4. Thermogravimetric analysis of $CsGaSe_3$ and $Cs_2Ga_2Se_5$ showing the measured TG curve (mid), the differential TG curve (top), and the respective DTA curve of the analysis (heating rate 4 °C/min, N_2 atmosphere).

calcd 9.9%) are in good agreement with the loss of one equivalent of selenium with regard to the respective chemical formula. Different heating rates in case of $Cs_2Ga_2Se_5$ resulted in slightly different mass losses and slightly shifted TG curves (Figures S1–S2). This observation can be attributed to the kinetics of the decomposition reaction as only the substance at the surface of the crystallites decomposes at the beginning. Furthermore, selenium released from the sample has to diffuse to the surface to be detected as mass loss. In the case of $CsGaSe_3$, it was not possible to separate the different decomposition steps; only a marginal step could be detected in this case. The residues in both cases were identified as $CsGaSe_2$-*mC*16 using qualitative X-ray diffraction.

Schematic Overview. In the last step, the reversibility of these thermal decomposition reactions was investigated. Contrary to the analogous sulfides, this reaction can be reversed by simple addition of elemental selenium to both polymorphs of $CsGaSe_2$ or $Cs_2Ga_2Se_5$, respectively. However, the samples have to be annealed for a longer time (at least one week) without a temperature gradient in short silica ampules to ensure a quantitative back-transformation. Using this method, $CsGaSe_3$ can be recovered by annealing at 500 °C, while well crystalline $Cs_2Ga_2Se_5$ can be recovered by annealing at 600 °C for several days with the respective amounts of selenium. This observation is in line with our experimental procedure for the synthesis of $Cs_2Ga_2Se_5$[7] which was obtained far above the decomposition temperature observed in the X-ray measurements (Figure 3). Figure 5 summarizes all possible pathways for the synthesis of these selenogallates. The results of the X-ray diffraction and thermogravimetric experiments, however, also indicate that significant thermodynamic and kinetic effects have to be accounted for during the synthesis of these selenogallates. Furthermore, this behavior is in contrast to the sulfides $Cs_2Ga_2S_5$ and $CsGaS_3$, which can solely be recovered using polysulfide melts. A possible explanation for these differences might be the higher vapor pressure of sulfur (boiling point T_B = 445 °C) as compared to elemental selenium (boiling point T_B = 685 °C), and the significant gain in entropy which leads to an irreversible decomposition of the sulfides. Similar to the analogous sulfides, even though the compounds $CsGaSe_3$,

DOI: 10.1021/acs.inorgchem.8b00324
Inorg. Chem. 2018, 57, 5292–5298

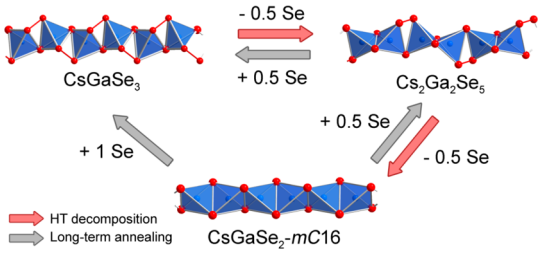

Figure 5. Schematic representation of possible pathways for the conversion of the selenogallates $CsGaSe_3$, $Cs_2Ga_2Se_5$, and $CsGaSe_2$ using the high-temperature decomposition route (red arrows) and long-term annealing after addition of the respective amount of selenium (gray arrows).

$Cs_2Ga_2Se_5$, and $CsGaSe_2$-*mC*16 appear related at first glance (similar anionic structures, unit cell dimensions, space groups), there is no crystallographic/mathematical strict symmetry relation between the crystal structures in terms of group−subgroup relation.

Thermal Expansion of $Cs_2Ga_2Se_5$, $CsGaSe_2$-mC64, and $CsGaSe_2$-mC16. As we obtained high quality synchrotron diffraction data for $Cs_2Ga_2Se_5$ and both polymorphs of $CsGaSe_2$, we decided to further investigate the behavior of the crystal structures at high temperatures. The unit cell volumes of all three compounds show a linear temperature dependence (Figure 6). Even though the volumes change

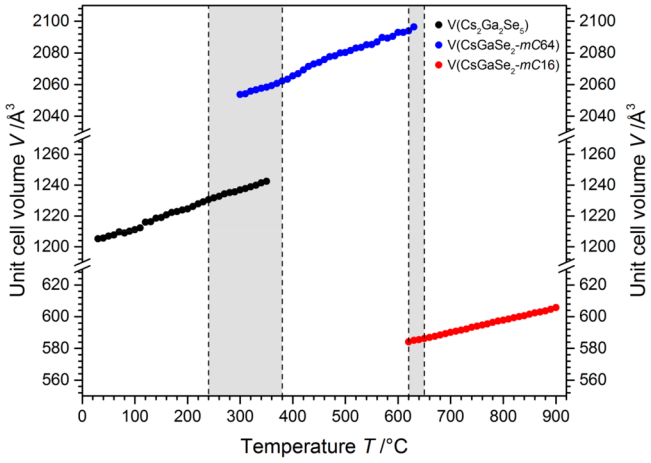

Figure 6. Plot of the unit cell volumes of $Cs_2Ga_2Se_5$ (black dots), $CsGaSe_2$-*mC64* (blue dots), and $CsGaSe_2$-*mC*16 (red dots) in the temperature region from room temperature to 900 °C. The gray shaded areas represent the two-phase regions. The estimated standard deviations are within the size of the data points and therefore not depicted.

linearly, significant discrepancies from the linear behavior can be observed for the cell axes and monoclinic angles in the two-phase regions. These discrepancies can be attributed to the drastic rearrangements of the atoms from chains $^1_\infty[Ga_2(Se_2)Se_3^{2-}]$ to layers $^2_\infty[Ga_4Se_8^{4-}]$ to chains $^1_\infty[GaSe_2^-]$ in these selenogallates. Plots of all unit cell parameters for the three compounds are provided in the Supporting Information (Figures S4−S6).

Table 2 lists the linear thermal expansion coefficients of $Cs_2Ga_2Se_5$, $CsGaSe_2$-*mC64*, and $CsGaSe_2$-*mC*16 which were determined from the slope of the respective graphs. Interestingly, the volumetric expansion coefficients of all three

Table 2. Thermal Linear (α) and Volumetric (γ) Expansion Coefficients of $Cs_2Ga_2Se_5$, $CsGaSe_2$-*mC64*, and $CsGaSe_2$-*mC16*

compound	$Cs_2Ga_2Se_5$	$CsGaSe_2$-*mC64*	$CsGaSe_2$-*mC16*
temperature region	30−240 °C	410−610 °C	660−900 °C
$\alpha(a)$ /Å °C^{1-}	$3.80(9) \times 10^{-4}$	$2.06(2) \times 10^{-4}$	$3.43(2) \times 10^{-4}$
$\alpha(b)$/Å °C^{1-}	$3.69(8) \times 10^{-4}$	$1.95(2) \times 10^{-4}$	$8.76(5) \times 10^{-4}$
$\alpha(c)$/Å °C^{1-}	$5.55(1) \times 10^{-4}$	$3.78(1) \times 10^{-4}$	$0.25(1) \times 10^{-4}$
$\gamma(V)$/Å^3 °C^{1-}	$1.22(2) \times 10^{-1}$	$1.30(3) \times 10^{-1}$	$0.77(1) \times 10^{-1}$

compounds are fairly similar to the layered compound $CsGaSe_2$-*mC64* showing the largest volume increase. Due to the different dimensionality of these selenogallates, the linear expansion coefficients of the unit cell parameters vary significantly. The anionic layers $^2_\infty[Ga_4Se_8^{4-}]$ in $CsGaSe_2$-*mC64* are isotropic in the *AB* plane, resulting in almost identical unit cell axes *a* and *b* and subsequently nearly identical linear expansion coefficients $\alpha(a)$ and $\alpha(b)$. For the quite anisotropic one-dimensional structures in $Cs_2Ga_2Se_5$ and $CsGaSe_2$-*mC*16, significant discrepancies in the expansion coefficients of the unit cell parameters are observed. Because the arrangement of the Cs^+ cations in both compounds is identical, these differences must stem from the different anionic selenogallate chains. Therefore, one would expect significant differences of the thermal expansion coefficients parallel and perpendicular to these chains, respectively. In $CsGaSe_2$-*mC*16, the *c*-axis represents the direction of the chains $^1_\infty[GaSe_2^-]$ in the crystal structure. The lengths of the *a*- and *b*-axes increase nearly 10- and 20-fold compared to the *c*-axis. In $Cs_2Ga_2Se_5$, the anionic chains $^1_\infty[Ga_2(Se_2)Se_3^{2-}]$ run along the crystallographic 101 direction. Therefore, no distinct simple statement linking the expansion coefficients and crystal structure can be made. However, a larger overall increase in the unit cell volumes can be observed in $Cs_2Ga_2Se_5$ as compared to $CsGaSe_2$-*mC*16.

Optical Properties. Like to the analogous sulfides, $CsGaSe_3$, $Cs_2Ga_2Se_5$, and $CsGaSe_2$-*mC*16 are semiconductors with optical band gaps reported as 2.25, 1.95, and 2.38 eV, respectively.[4,7,21] In the course of our investigations, we first redetermined the optical band gaps of all three selenogallates, which are listed in Table 3. A value of 2.17 eV for $CsGaSe_3$ is in

Table 3. Experimental and Calculated Optical Band Gaps of $CsGaSe_3$, $Cs_2Ga_2Se_5$, and $CsGaSe_2$-*mC16*

compound	experimental value E_g^{exp}/eV	calculated value E_g^{calc}/eV
$CsGaSe_3$	2.17	1.69
$Cs_2Ga_2Se_5$	2.08	2.06
$CsGaSe_2$-*mC16*	2.36	2.54

good agreement with the value of 2.25 eV reported by Kanatzidis[4] and the reddish brown color of the powdered sample. For the sulfides, a strong connection between the number of disulfide units in the anionic structures and the optical band gaps was observed. An increasing amount of these S_2^{2-} units in the system $Cs_2[Ga_2(S_2)_{2-x}S_{2+x}]$ (x = 0, 1, 2) leads to a decrease of the optical band gaps from 3.27 eV in $CsGaS_2$-*mC*16 to 2.78 eV in $CsGaS_3$. This observation is also made in the system $Cs_2[Ga_2(Se_2)_{2-x}Se_{2+x}]$ (x = 0, 1, 2). However, due to the significantly smaller band gaps, the selenides can absorb light in the visible spectrum, making them interesting materials for different applications, e.g., chemical photocatalysis. To further study the electronic properties and bonding situation in

DOI: 10.1021/acs.inorgchem.8b00324
Inorg. Chem. 2018, 57, 5292−5298

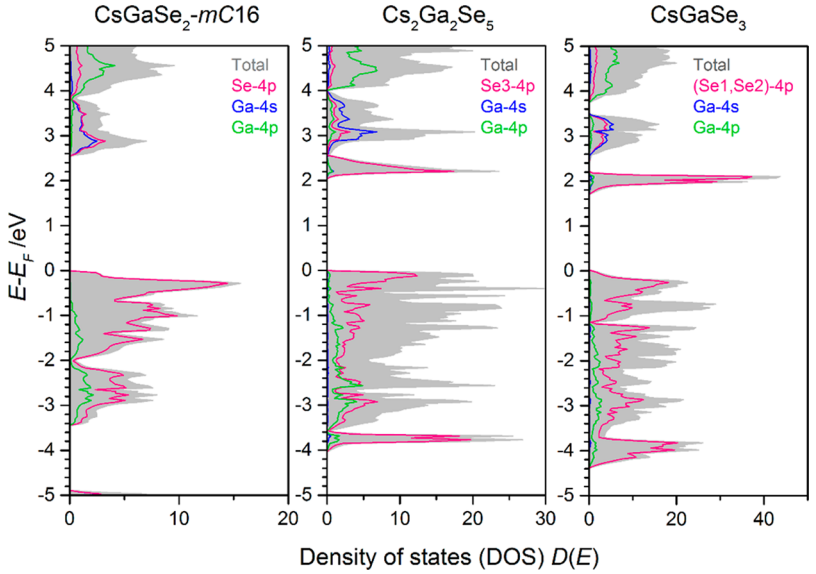

Figure 7. Calculated total (TDOS, gray) and orbital projected density of states (PDOS, colored lines) near the band gaps, revealing lower energies of the Se 4p states of the Se_2^{2-} units in $Cs_2Ga_2Se_5$ (Se3 site) and $CsGaSe_3$ (Se1 and Se2 sites).

the title compounds, we performed relativistic DFT calculations. The orbital projected density of states (PDOS) near the band gaps for $CsGaSe_2$-*mC*16, $Cs_2Ga_2Se_5$, and $CsGaSe_3$ are shown in Figure 7. These calculated band gaps are in good agreement with the experimentally determined values (Table 3). Figure S7 shows the band structures of the three direct band gap semiconductors as well as the respective DOS in the range from $-8.5\ \text{eV} \leq E-E_F \leq +5.0\ \text{eV}$.

Similar to other chalcogenotrielates investigated by us[6,17,18,21−23] or other groups,[24,25] the alkali metal does not significantly influence the optical band gaps of these compounds, as the unoccupied Cs-6*s* states indicate a mainly ionic bonding between Cs^+ and the chalcogenometalate units. Interactions of gallium and selenium within the $GaSe_4$ tetrahedra lead to a splitting into valence and conduction band. The states below and above the band gap are dominated by the Se 4p states in case of the compounds containing Se_2^{2-} dumbbells. Like in the related sulfides $CsGaS_2$-*mC*16, $Cs_2Ga_2S_5$, and $CsGaS_3$, the absence of diselenide units significantly widens the band gap in $CsGaSe_2$-*mC*16.[17] In $Cs_2Ga_2Se_5$ and $CsGaSe_3$, these Se_2^{2-} units, due to their reduced charge, form weaker ionic Ga−Se interactions, thus leading to smaller band gaps due to the lower energies of the unoccupied Se 4p states of the Se_2^{2-} units. These weaker interactions further result in longer distances *d*(Ga−Se) between Ga^{3+} and the coordinating atoms of the Se_2^{2-} units in $Cs_2Ga_2Se_5$ and $CsGaSe_3$. Furthermore, the covalent Ga−Se interactions are weaker in the compounds containing Se_2^{2-} units, which can also be observed in the Raman spectra (Figure S5). These show a blue shift of the Ga−Se stretching modes with increasing Se_2^{2-} content. In analogy to the sulfides, an increasing number of diselenide moieties only slightly reduce the band gaps. Furthermore, the search for the formation of a possible solid solutions series $Cs_2Ga_2Se_{4+x}$ (x = 0−2) always resulted in a phase separation into $Cs_2Ga_2Se_5$ and either $CsGaSe_2$ or $CsGaSe_3$ and no significant changes in the band gaps of these phases.

CONCLUSION

In this work, we investigated the thermal behavior of the selenogallates $CsGaSe_3$ and $Cs_2Ga_2Se_5$. These selenides release gaseous chalcogen upon heating, similar to the analogous sulfides $CsGaS_3$ and $Cs_2Ga_2S_5$. In situ X-ray diffraction and thermogravimetric experiments revealed a stepwise degradation of $CsGaSe_3$ to $Cs_2Ga_2Se_5$ and then to $CsGaSe_2$-*mC*16. During each step, one diselenide unit of the anionic chains $^1_\infty[Ga_2(Se_2)_{2-x}Se_{2+x}^{2-}]$ (x = 0, 1, 2) decomposes, and one equivalent of selenium is released. This degradation can be reversed by addition of elemental selenium and long-term annealing of the samples at the respective temperatures contrary to the sulfide phases. An analysis of the band gaps in these compounds revealed decreasing optical band gaps with increasing Se_2^{2-} content. The desired formation of a wide range solid solutions and a subsequent tailoring of the optical band gaps in this system, however, were not observed.

EXPERIMENTAL SECTION

Synthesis of the Starting Materials. GaSe was prepared by a chemical vapor transport reaction from gallium (Chempur 99.99%) and selenium (Chempur 99.999%) using iodine (Sigma-Aldrich 99.8%) as transporting agent.[26] Cesium azide CsN_3 was synthesized by passing a diluted stream of hydrazoic acid (prepared by acidifying of an aqueous solution of NaN_3 (Sigma-Aldrich 99.0%)) into an aqueous solution of Cs_2CO_3 (Rockwood-Lithium 99.9%).[27] Thus, destillation and handling of highly reactive elemental cesium can be avoided. *Attention*: Condensed HN_3 is highly explosive. Tools made from transition metals must be avoided.

Synthesis of $CsGaSe_3$ and $Cs_2Ga_2Se_5$. The ternary selenogallates $CsGaSe_3$ and $Cs_2Ga_2Se_5$ were synthesized by controlled thermal decomposition (0.2 g batch size, heating rate 0.5 °C/min) of CsN_3 mixed with stoichiometric amounts of GaSe and selenium in a quartz glass ampule under dynamic vacuum conditions. Upon heating, the azide decomposes to the pure alkali metal, which immediately reacts with the other starting materials, resulting in the formation of an inhomogeneous raw product. Flame-sealed ampules containing these raw products were annealed at 600 °C for $Cs_2Ga_2Se_5$[7] and at 500 °C for $CsGaSe_3$.[4]

X-ray Powder Diffraction. The in situ high-temperature X-ray diffraction experiments on $CsGaSe_3$ were performed on a STOE Stadi P diffractometer using monochromatized Mo $K\alpha_1$ radiation (Ge[111] monochromator, λ = 0.709300 Å). The air sensitive powdered samples were flame-sealed in 0.3 mm quartz glass capillaries which were placed in another 0.5 mm quartz glass capillary due to the furnace

DOI: 10.1021/acs.inorgchem.8b00324
Inorg. Chem. 2018, 57, 5292−5298

architecture. A STOE capillary furnace 0.65 was used as high-temperature unit. The furnace temperature was controlled by a Eurotherm 24.16 controller ($\Delta T = \pm 1$ °C) and the WinX^{POW} software package from STOE & Cie was used for data collection and processing.[28] The diffraction experiments using synchrotron radiation were performed at the ID-22 beamline of the European Synchrotron Radiation Facility (ESRF) using a custom wavelength of $\lambda = 0.399949$ Å. The powdered samples were loaded in flame-sealed 0.7 mm quartz glass capillaries. A Cyberstar hot-air blower was used as high-temperature unit, and the reflection intensities were detected by a nine-crystal multianalyzer bank. All diffraction patterns were analyzed by using LeBail fits in Jana2006.[29] The initial unit cell parameters for each refinement were determined using common indexing programs like ITO[30] or TREOR[31] implemented in WinX^{POW}.[28] For the LeBail fit of the discussed selenogallates, a manual background combined with 3 Legendre polynoms was used. The reflection profiles were described by pseudo Voigt functions refining the parameters GW, GU, LY, and LX. An exemplary LeBail fit (including the difference plot) of $Cs_2Ga_2Se_5$, $CsGaSe_2$-*mC*64, and $CsGaSe_2$-*mC*16 can be found in Figure S3.

Differential Thermal Analysis and Thermogravimetry (DTA-TG). DTA-TG measurements were performed in a dynamic nitrogen atmosphere in Al_2O_3 crucibles using a STA PT 1000 thermobalance from Linseis. The instrument was calibrated using standard reference materials.

UV/Vis Spectroscopy. The diffuse reflectance measurements were performed on a Bruins Omega 20 UV/vis spectrometer using $BaSO_4$ as white standard (100% reflectance). The absorption data were calculated from the reflectance spectra using a modified Kubelka–Munk function.[32,33]

DFT Calculations. First-principle calculations were performed within the framework of DFT using exchange-correlation functionals in the generalized gradient approximation (GGA) according to Perdew–Burke–Ernzerhof (PBE).[34] For the calculation of the total energies and band structures, the full-potential local-orbital code FPLO14 was applied.[35] A *k*-grid mesh of 12 × 12 × 12 was used. The calculations converged with a maximum divergence of $<10^{-7}$ Hartree.

■ ASSOCIATED CONTENT

Supporting Information

The Supporting Information is available free of charge on the ACS Publications website at DOI: 10.1021/acs.inorgchem.8b00324.

TGA analysis of $Cs_2Ga_2Se_5$ with different heating rates; LeBail fits of $Cs_2Ga_2Se_5$, $CsGaSe_2$-*mC*64, and $CsGaSe_2$-*mC*16; plots of the unit cell parameters of $Cs_2Ga_2Se_5$, $CsGaSe_2$-*mC*64, and $CsGaSe_2$-*mC*16 at different temperatures; band structure plots and respective DOS for $CsGaSe_2$-*mC*16, $Cs_2Ga_2Se_5$, and $CsGaSe_3$; Raman spectra of $CsGaSe_2$-*mC*16, $Cs_2Ga_2Se_5$, and $CsGaSe_3$ (PDF)

■ AUTHOR INFORMATION

Corresponding Author

*E-mail: arno.pfitzner@chemie.uni-regensburg.de.

ORCID

Daniel Friedrich: 0000-0001-6953-8114

Christian Näther: 0000-0001-8741-6508

Arno Pfitzner: 0000-0001-8653-7439

Present Address

†C.N.: Institut für Anorganische Chemie, Christian-Albrechts-Universität zu Kiel, Olshausenstrasse 40, 24098 Kiel, Germany.

Notes

The authors declare no competing financial interest.

■ ACKNOWLEDGMENTS

The authors would like to thank Dr. Andy Fitch and his team for technical assistance during the X-ray measurements at ID-22 of the ESRF. We also like to express our gratitude to Rockwood-Lithium GmbH for generously supplying cesium carbonate and Prof. Dr. Manfred Scheer (University of Regensburg) for the Raman measurements.

■ REFERENCES

(1) Petrov, V.; Yelisseyev, A.; Isaenko, L.; Lobanov, S.; Titov, A.; Zondy, J. J. Second harmonic generation and optical parametric amplification in the mid-IR with orthorhombic biaxial crystals $LiGaS_2$ and $LiGaSe_2$. *Appl. Phys. B: Lasers Opt.* **2004**, *78*, 543–546.

(2) Isaenko, L.; Krinitsin, P.; Vedenyapin, V.; Yelisseyev, A.; Merkulov, A.; Zondy, J. J.; Petrov, V. A New Highly Nonlinear Chalcopyrite Optical Crystal for the Mid-IR. *Cryst. Growth Des.* **2005**, *5*, 1325–1329.

(3) Deiseroth, H. J.; Reiner, C. KIn_5S_6 und MIn_5S_7 (M = Na, K): Drei neue gemischtvalente Thioindate der Alkalimetalle und ihre kristallchemischen Beziehungen. *Z. Anorg. Allg. Chem.* **1998**, *624*, 1839–1845.

(4) Do, J.; Kanatzidis, M. G. The One-dimensional Polyselenide Compound $CsGaSe_3$. *Z. Anorg. Allg. Chem.* **2003**, *629*, 621–624.

(5) Suseela Devi, M.; Vidyasagar, K. Molten flux synthesis, single crystal X-ray structure and ion-exchange property of the first polythiogallate, $CsGaS_3$. *J. Chem. Soc., Dalton Trans.* **2002**, 4751–4754.

(6) Friedrich, D.; Pielnhofer, F.; Schlosser, M.; Weihrich, R.; Pfitzner, A. Synthesis, Structural Characterization, and Physical Properties of $Cs_2Ga_2S_5$, and Redetermination of the Crystal Structure of Cs_2S_6. *Chem. - Eur. J.* **2015**, *21*, 1811–1817.

(7) Friedrich, D.; Schlosser, M.; Pfitzner, A. Synthesis and Structural Characterization of $Cs_2Ga_2Se_5$. *Z. Anorg. Allg. Chem.* **2014**, *640*, 826–829.

(8) Eisenmann, B.; Jäger, J. Crystal structure of caesium catena-tritelluroaluminate, $CsAlTe_3$. *Z. Kristallogr.* **1991**, *197*, 251–252.

(9) Hammerschmidt, A.; Küper, J.; Stork, L.; Krebs, B. $Na_2B_2Se_7$, $K_2B_2S_7$ und $K_2B_2Se_7$: Drei Perchalkogenoborate mit neuem polymeren Anionengerüst. *Z. Anorg. Allg. Chem.* **1994**, *620*, 1898–1904.

(10) Lindemann, A.; Küper, J.; Hamann, W.; Kuchinke, D.; Köster, C.; Krebs, B. Syntheses, Crystal Structures, and Properties of the Three Novel Perselenoborates $RbBSe_3$, $CsBSe_3$, and $TlBSe_3$ with Polymeric Chain Anions. *J. Solid State Chem.* **2001**, *157*, 206–212.

(11) Püttmann, C.; Hiltmann, F.; Hamann, W.; Brendel, C.; Krebs, B. Die Perthioborate $RbBS_3$, $TlBS_3$ und $Tl_3B_3S_{10}$. *Z. Anorg. Allg. Chem.* **1993**, *619*, 109–116.

(12) Sheldrick, W. S.; Wachhold, M. Crystal structure of potassium selenidoantimonate(III), $K_2Sb_4Se_8$. *Z. Kristallogr. - New Cryst. Struct.* **1998**, *213*, 25.

(13) Chen, Z.; Li, G.-Q.; Chen, R.-Y.; Zheng, X.; Huang, Z.-X. Solvothermal synthesis and crystal structure of metal chalcogenide $CsSb_2(Se_2)_{0.5}Se_3$. *Wuji Huaxue Xuebao* **2006**, *22*, 27–30.

(14) Sheldrick, W. S.; Wachhold, M. Crystal structure of rubidium selenidoantimonate(III), $Rb_2Sb_4Se_8$. *Z. Kristallogr. - New Cryst. Struct.* **1998**, *213*, 24.

(15) McCarthy, T. J.; Kanatzidis, M. G. Polysulfide Ligands in Solid-State Antimony Compounds. Isolation and Structural Characterization of $Cs_2Sb_4S_8$ and $CsSbS_6$. *Inorg. Chem.* **1994**, *33*, 1205–1211.

(16) Rödl, T.; Weihrich, R.; Wack, J.; Senker, J.; Pfitzner, A. Rational Syntheses and Structural Characterization of Sulfur-Rich Phosphorus Polysulfides: α-P_2S_7 and β-P_2S_7. *Angew. Chem., Int. Ed.* **2011**, *50*, 10996–11000.

(17) Friedrich, D.; Schlosser, M.; Pfitzner, A. Interconversion of One-Dimensional Thiogallates $Cs_2[Ga_2(S_2)_{2-x}S_{2+x}]$ (x = 0, 1, 2) by Using High-Temperature Decomposition and Polysulfide-Flux Reactions. *Cryst. Growth Des.* **2017**, *17*, 4887–4892.

(18) Friedrich, D.; Schlosser, M.; Weihrich, R.; Pfitzner, A. Polymorphism of $CsGaS_2$ - structural characterization of a new two-

DOI: 10.1021/acs.inorgchem.8b00324
Inorg. Chem. 2018, 57, 5292–5298

dimensional polymorph and study of the phase-transition kinetics. *Inorg. Chem. Front.* **2017**, *4*, 393−400.
(19) Schmitz, D.; Bronger, W. Die Kristallstruktur von $CsGaS_2$. *Z. Naturforsch., B: J. Chem. Sci.* **1975**, *30B*, 491−493.
(20) Deiseroth, H. J. Ungewöhnliche lineare, oligomere Anionen $(Ga_nSe_{2n+2})^{(n+4)-}$ (n = 2, 4, 6) in festen Selenogallaten des Cäsiums. *Z. Kristallogr.* **1984**, *166*, 283−295.
(21) Friedrich, D.; Schlosser, M.; Pfitzner, A. Synthesis, Crystal Structure, and Physical Properties of Two Polymorphs of $CsGaSe_2$, and High-Temperature X-ray Diffraction Study of the Phase Transition Kinetics. *Cryst. Growth Des.* **2016**, *16*, 3983−3992.
(22) Friedrich, D.; Schlosser, M.; Pfitzner, A. Synthesis and Structural Characterization of the layered Selenogallate $RbGaSe_2$. *Z. Anorg. Allg. Chem.* **2017**, *643*, 1589−1592.
(23) Friedrich, D.; Schlosser, M.; Etter, M.; Pfitzner, A. Influence of Alkali Metal Substitution on the Phase Transition Behavior of $CsGaQ_2$ (Q = S, Se). *Crystals* **2017**, *7*, 379.
(24) Feng, K.; Mei, D.; Bai, L.; Lin, Z.; Yao, J.; Wu, Y. Synthesis, structure, physical properties, and electronic structure of $KGaSe_2$. *Solid State Sci.* **2012**, *14*, 1152−1156.
(25) Benmakhlouf, A.; Bentabet, A.; Bouhemadou, A.; Maabed, S.; Khenata, R.; Bin-Omran, S. Structural, elastic, electronic and optical properties of $KAlQ_2$ (Q = Se, Te): A DFT study. *Solid State Sci.* **2015**, *48*, 72−81.
(26) Ishii, T.; Kambe, N. GaSe single crystal growth by iodine vapor transport. *J. Cryst. Growth* **1986**, *76*, 489−493.
(27) Suhrmann, R.; Clusius, K. Über die Reindarstellung der Alkalimetalle. *Z. Anorg. Allg. Chem.* **1926**, *152*, 52−58.
(28) *STOE WinX^{POW}*, version 3.10; STOE & Cie GmbH: Darmstadt, 2016.
(29) Petricek, V.; Dusek, M.; Palatinus, L. Crystallographic Computing System JANA2006: General features. *Z. Kristallogr. - Cryst. Mater.* **2014**, *229*, 345.
(30) Visser, J. A fully automatic program for finding the unit cell from powder data. *J. Appl. Crystallogr.* **1969**, *2*, 89−95.
(31) Boultif, A.; Louer, D. Indexing of powder diffraction patterns for low-symmetry lattices by the successive dichotomy method. *J. Appl. Crystallogr.* **1991**, *24*, 987−993.
(32) Kubelka, P.; Munk, F. Ein Beitrag zur Optik der Farbanstriche. *Z. tech. Phys.* **1931**, 593.
(33) Kisch, H. Semiconductor Photocatalysis—Mechanistic and Synthetic Aspects. *Angew. Chem., Int. Ed.* **2013**, *52*, 812−847.
(34) Perdew, J. P.; Burke, K.; Ernzerhof, M. Generalized Gradient Approximation Made Simple. *Phys. Rev. Lett.* **1996**, *77*, 3865−3868.
(35) Koepernik, K.; Eschrig, H. Full-potential nonorthogonal local-orbital minimum-basis band-structure scheme. *Phys. Rev. B: Condens. Matter Mater. Phys.* **1999**, *59*, 1743−1757.

DOI: 10.1021/acs.inorgchem.8b00324
Inorg. Chem. 2018, 57, 5292−5298